

# 1 **Ferrovulcanism: Iron Volcanism on Metallic Asteroids**

2 **Jacob N. H. Abrahams<sup>1</sup>, Francis Nimmo<sup>1</sup>**

3 <sup>1</sup>Department of Earth and Planetary Science, University of California Santa Cruz, Santa Cruz, CA 95064

## 4 **Key Points:**

- 5 • Metallic asteroids begin fully molten, and as they solidify their remaining melt is  
6 buoyant.
- 7 • The primary stress state of metallic asteroid crust is compression, limiting the abil-  
8 ity of melt at depth to reach the surface.
- 9 • Local stress changes likely allow this compression to be overcome, and we predict  
10 metallic asteroids should host volcanic activity.

---

Corresponding author: Jacob Abrahams, [abrahams@ucsc.edu](mailto:abrahams@ucsc.edu)

## Abstract

Metallic asteroids, the exposed cores of disrupted planetesimals, are expected to have been exposed while still molten. Some would have cooled from the outside in, crystallizing a surface crust which would then grow inward. Because the growing crust is expected to be more dense than the underlying melt, this melt will tend to migrate toward the surface whenever it is able. Compressional stresses produced in the crust while it cools will be relieved locally by thrust faulting, which will also provide potential conduits for melt to reach the surface. We predict iron volcanism to have occurred on metallic asteroids as they cooled and discuss the implications of this process for both the evolution and the modern appearance of these bodies.

## 1 Introduction

Three major types of crustal material are observed in the solar system. The most familiar, silicate crust, is found on the terrestrial planets and their moons, most asteroids, and on Io. The other common type of crust is formed from ices, primarily water ice, on the surfaces of most outer solar system moons, some asteroids, and most Kuiper belt objects. In addition to ice and silicates, a less common third type of crust is present in the solar system: metallic core material left behind following collisional disruption of the mantle of a differentiated body (Asphaug et al., 2006; Yang et al., 2007). These bodies have been detected in the asteroid belt (Matter et al., 2013; Neeley et al., 2014) and contribute substantially to the meteorite record (Hutchison, 2004). However, our understanding of their surfaces is very limited – the first detailed images of a metallic asteroid will come from the Psyche spacecraft, which is scheduled to launch in 2022 (Lord et al., 2017).

Volcanism occurs throughout the solar system in a variety of different forms (e.g. Lopes & Gregg, 2004; Wilson, 2009). All terrestrial planets (and Io) exhibit silicate volcanism, and a number of icy bodies display either geomorphic signs of cryovolcanism (Moore et al., 2016; Schenk et al., 2001) or directly observed plume behavior (Porco et al., 2006; Roth et al., 2014). In this paper we explore the question of whether metallic bodies can host their own novel style of volcanism. Metallic volcanism should bear most resemblance to silicate volcanism, where the melt is buoyant relative to the solid matrix. This is in contrast to cryovolcanism, where the melt is more dense and mechanisms other than buoyancy are needed to aid its ascent (e.g. Crawford & Stevenson, 1988; Manga & Wang, 2007). The main differences between iron volcanism and silicate volcanism are the lower viscosity of liquid metal, the higher ductility of solid metal, metal’s higher resistance to fracture and the likely absence of a low-density metallic crust able to stall fluid migration. In addition, our analysis is concerned with a body hosting an iron ‘magma ocean’, where the entire interior is molten, rather than broad regions of low melt fraction or magma confined to small chambers.

All but the smallest differentiated bodies will have partially molten iron cores for at least the first  $\sim 100$  million years of the solar system, the period in which their mantles are most likely to be removed (Bottke et al., 2005). When a fully molten core is then exposed to space, it will rapidly form a quench crust on the surface. This new crust will either sink, exposing new melt to space and rapidly freezing the whole body, or it will be supported by its own strength and crystallize slowly from the outside in. Crucially, observations of cooling rate-Ni correlations indicate that some asteroid bodies crystallize from the outside-in (Chabot & Haack, 2006; Yang et al., 2007, 2008), which is the mode of solidification of interest to this work. These observations show that, within the IVA meteorite family, the samples with the fastest cooling rates have the lowest incompatible element contents, implying that the shallowest material crystallizes first i.e. top-down solidification. While this explanation is not universally accepted (Albarède et al., 2013), for the purpose of this paper we assume it is correct; further aspects of solidifi-

62 cation are addressed in Scheinberg et al. (2016) and Neufeld et al. (2019). We predict  
 63 that in such bodies the buoyant melt beneath the crust will periodically be able to erupt,  
 64 influencing their cooling and creating volcanic features on the surface.

65 The aim of this manuscript is to investigate the basics of metallic volcanism. Be-  
 66 cause iron volcanism is a novel concept, and many of the important parameters are poorly  
 67 constrained, we take an order-of-magnitude approach whenever possible and are only seek-  
 68 ing to make approximate predictions for the real behavior. First we discuss the thermal  
 69 and mechanical evolution of an initially molten metallic asteroid. Then we address the  
 70 ability of melt to reach the surface and challenges to that migration. We conclude by  
 71 discussing some features of how metallic volcanism may present itself, and the need for  
 72 continuing work anticipating its morphology, looking for it in current records, and col-  
 73 lecting additional data.

## 74 2 Thermal Evolution

### 75 2.1 Thermal evolution prior to disruption

76 Bodies formed in the first  $\sim 2.5$  Myr of the solar system will possess enough short  
 77 lived radionuclides, particularly  $^{26}\text{Al}$ , to melt and separate metals and silicates (Gold-  
 78 stein et al., 2009; Hevey & Sanders, 2006). In the absence of mantle convection (Tkalcic  
 79 et al., 2013) or silicate melt advection, the core will not begin to cool significantly un-  
 80 til a conductive cooling wave has propagated to the base of the mantle. For a thermal  
 81 diffusivity of  $\approx 10^{-6}$  m<sup>2</sup>/s (Carslaw & Jaeger, 1959), even a 60 km mantle has a ther-  
 82 mal timescale of 100 Myr. Since 16 Psyche, the largest metallic asteroid, has an aver-  
 83 age radius over 100 km (Shepherd et al., 2017) its mantle thermal timescale prior to dis-  
 84 ruption will have exceeded this value. Because disruption most likely occurred during  
 85 terrestrial planet accretion (Bottke et al., 2005), the cores of proto-Psyche and other similar-  
 86 sized asteroids will have been molten when disruption occurred.

### 87 2.2 Thermal evolution after disruption

88 After disruption (and any requisite reaccretion, which will be rapid - on orbital timescales)  
 89 the body of interest will be a molten, hydrostatic spheroid exposed to space. Initially,  
 90 a quench crust will form very rapidly—a millimeter thick crust can form in  $\sim$ minutes—  
 91 but crustal growth slows down substantially once conduction replaces radiation as the  
 92 rate-limiting step. Preventing fresh crust from immediately sinking until a self-supporting  
 93 crust can form is beyond the scope of this paper, but as discussed in Section 1, the me-  
 94 teorite record suggests that this took place on some metallic bodies. Moreover, crystal-  
 95 lization from the top down, rather than from the bottom up, is expected based on the  
 96 expected liquidus and adiabat slopes (Williams, 2009). Once a strong crust forms, in the  
 97 absence of core superheat and volcanism its thickness  $h$  will grow according to the Ste-  
 98 fan solution (Turcotte & Schubert, 2014), approximated by  $h \approx 20 \text{ km}(t/1 \text{ Myr})^{1/2}$ .  
 99 For these very approximate values, the time to form a 20 km crust is roughly one Myr.

100 This evolution can be more complicated if the simple top-down conductive cool-  
 101 ing of the Stefan problem does not apply (Scheinberg et al., 2016). Advection is one way  
 102 to modify this picture, but as discussed later fluid eruption is not expected to significantly  
 103 alter the thermal behavior. Delamination at the base of the crust can also modify the  
 104 thermal evolution of the body by maintaining a thinner crust. However, although de-  
 105 lamination is likely to occur, Neufeld et al. (2019) show that neither it nor core super-  
 106 heat significantly modify the overall thermal evolution of the body, and that the Stefan  
 107 assumption is generally justified.

### 108 3 Volcanic Cycle

109 Having discussed thermal evolution, we now move on to a discussion of how metallic  
 110 volcanism might arise. The eruption process we describe takes place in three major  
 111 stages, depicted in cartoon form in Figure 1. As the crust solidifies, the decrease in vol-  
 112 ume associated with the phase change results in radial contraction and compression. The  
 113 second stage occurs when this stress exceeds the friction on existing faults, those faults  
 114 move, and local low-stress regions surrounding the faults arise. The interior melt is then  
 115 able to force open these cracks and migrate through them. The third stage describes when  
 116 the liquid interior, which now has a decreased volume, causes sufficient contraction to  
 117 close the cracks again and re-establish local compression.

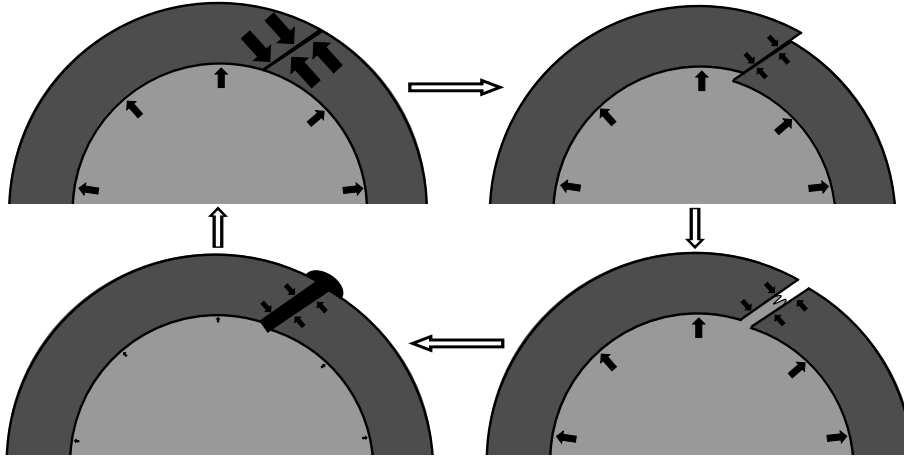


**Figure 1.** Cartoon depicting the volcanic cycle we describe. Beginning in the top-left is the typical state of the crust, where compressional stress prevents the melt at depth from reaching the surface. Volcanism then begins with a faulting event and the resulting decreased local compressional stress in the crust is no longer larger than hydrostatic pressure. Next, the liquid interior forces open the fault and melt migrates through the newly formed dike. Finally, melt reaches the surface and the now-depressurized ocean is no longer able to support the crust, causing the crack to close again. Subsequent crustal growth increases contraction in the crust slowly until faulting can occur again.

#### 118 3.1 Stage 1: Stress evolution due to bulk solidification

119 New solid will occupy a smaller volume than the melt from which it formed, and  
 120 the resulting radial contraction generates compression. The deeper, hotter solid (the deeper  
 121  $\sim$ half of the crust) will be ductile and able to viscously relax away this stress, while the  
 122 colder upper layers will either deform elastically or undergo brittle failure. Because the  
 123 crust will be in compression, volcanism will tend to be suppressed. To erupt, melt needs  
 124 to force open cracks which are being held together by compressive stresses. It is impor-  
 125 tant to note that both Mercury and the Moon host volcanism despite globally compressive  
 126 stress environments (Head & Wilson, 1992; Klimczak et al., 2018), so silicate vol-  
 127 canism can - at least locally and temporarily - overcome compression.

128 For a nominal 10 km crust with a linear thermal gradient, that gradient is  $\frac{dT}{dz} \approx$   
 129  $10^{-1}$  K/m. This corresponds to a radial contraction (due to crystallization) of  $h \frac{\Delta\rho}{\rho} =$

130  $\frac{k \frac{dT}{dz}}{L\rho} \frac{\Delta\rho}{\rho} \approx 10^{-10}$  m/s, where  $L$  is latent heat and  $k$  is thermal conductivity. Note that  
 131 part of the contraction is due to the entire crust cooling as the thermal profile gets longer,  
 132 which has a similar magnitude to the contraction due to crystallizing so we fold it into  
 133 our already very approximate  $\Delta\rho$ . This volume loss corresponds to a strain rate of  $\dot{\epsilon} =$   
 134  $\dot{h} \frac{\Delta\rho}{\rho} / R \sim 10^{-15}$  s $^{-1}$ . This strain rate will evolve substantially with the crustal thick-  
 135 ness; output from a simple numerical model of solidification-derived strain yields com-  
 136 parable results and is depicted in Figure 2.

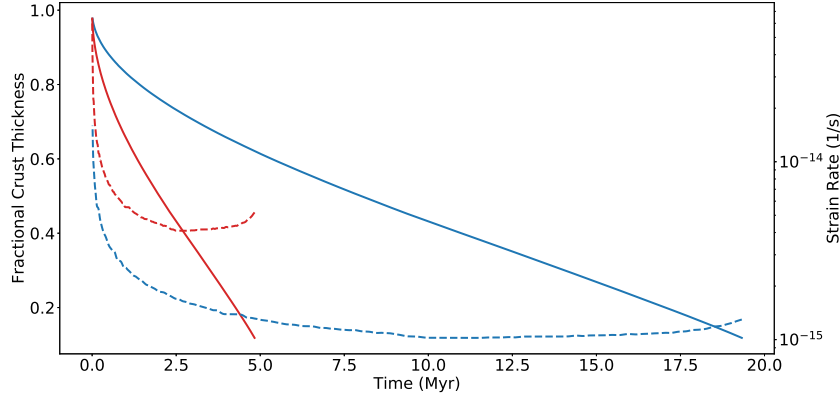


**Figure 2.** Evolution of an initially molten spherical iron body. Solid lines show the thickness of solid crust as a fraction of body radius and dashed lines show smoothed strain rate due to surface contraction. Red lines are for a 100 km radius body and blue lines are for a 200 km radius body. This model uses the approach of Nimmo & Spencer (2015) to numerically solve the Stefan problem with the surface pinned to 200 K, the liquid interior at 1200 K and other parameter values given in Table 1. Models taking core superheat and delamination into account (Neufeld et al., 2019) yield similar results

## 137 3.2 Stage 2: Dike Formation

### 138 3.2.1 Dike Opening in Brittle Crust by Magma Ocean Overpressure

139 Light fluid underlying a dense crust will experience an upwards buoyancy pressure.  
 140 This pressure is given by

$$141 P_{ex} = gh\Delta\rho \quad (1)$$

142 where  $h$  is the thickness of the crust and  $\Delta\rho$  is the density contrast between the crust  
 143 and the liquid interior. This quantity is likely of order a few percent of  $\rho$  and is a com-  
 144 bination of contraction due to crystallization, contraction due to cooling, and light el-  
 145 ement exclusion during crystallization. For an eruption to occur, this excess pressure must  
 146 exceed compressional stresses in the elastic crust. Assuming the crust is already frac-  
 147 tured, the stress to move a lithospheric fault (i.e. the maximum differential stress that  
 148 can be present in the lithosphere) for the nominal crustal thickness of 10 km is given by  
 149 Turcotte & Schubert (2014)

$$150 \sigma_{max} = \frac{2f_s\rho gh}{(1 + f_s^2)^{1/2} - f_s} \quad (2)$$

$$151 \approx \frac{\rho}{4} gh \approx 2 \text{ MPa} \quad (3)$$

152 where  $f_s \approx 0.65$  is the coefficient of friction on crustal faults. This indicates that the  
 153 lithosphere is able to support compressional stresses about  $\frac{\rho/\Delta\rho}{\Delta\rho} \approx 10$  times larger than  
 154 the excess hydrostatic pressure produced by its weight on the molten interior. However,  
 155 contraction can easily exceed this stress and cause faults to fail. With  $E$  as Young's Mod-  
 156 ulus, the strain required is  $\frac{\sigma_{max}}{E} \approx \frac{2 \times 10^6}{10^{11}} = 2 \times 10^{-5}$ , which accumulates in  $\frac{2 \times 10^{-5}}{10^{-15} \text{ s}^{-1}} \approx$   
 157 1 kyr, so faults will frequently move and relieve stress. Assuming that fault motion is  
 158 able to relieve most of the accumulated stress (Fulton et al., 2013) within a local area,  
 159 the excess fluid pressure can then force cracks open during such periods.

### 160 *3.2.2 Fracture Initiation in Ductile Crust*

161 We argued above that melt ascent through the brittle section of the crust is pos-  
 162 sible, locally and temporarily, despite the overall compressional stress environment. How-  
 163 ever, the melt needs to be able to first ascend into the brittle region of the crust, which  
 164 requires propagation through the nominally ductile lower crust. If partial melt is present  
 165 in this region, porous flow may feed shallower, macroscopic dikes (Rubin, 1998). Below  
 166 we will discuss the initiation of fractures at (or near) the base of the crust in the absence  
 167 of partial melt, and then their ability to propagate under the influence of inflowing melt.

168 One problem that has to be overcome to form a fracture is the ductility of the iron  
 169 near the base of the crust. Near its melting point, solid iron has a viscosity of  $\sim 10^{11} \text{ Pa} \cdot \text{s}$   
 170 (Frost & Ashby, 1982) and thus a viscoelastic response (Maxwell) timescale of 1 s, so  
 171 for it to respond in a brittle fashion, the strain rate has to exceed  $1 \text{ s}^{-1}$ . The other ma-  
 172 jor difficulty is the fact that iron has a high tensile strength, on the order of 100 MPa  
 173 (Ashby, 1999, Figure 4.4), so large stresses are needed for fractures to form. These fac-  
 174 tors make fracture propagation much more challenging than the equivalent problem in  
 175 silicate settings (Jellinek & DePaolo, 2003; Karlstrom & Richards, 2011, e.g.).

176 The most likely way to generate large stresses quickly is from cratering. Peak pres-  
 177 sures on the order of hundreds of MPa occur to depths of 10 to 100 times the impactor  
 178 radius, depending on the impact velocity (Melosh, 1989, Section 5.2). Thus, for impactors  
 179 with radii around 1 km, fractures should extend through to the base of the crust while  
 180 it is still only tens of kilometers thick. The role of impacts in volcanism is observed else-  
 181 where in the solar system, particularly on Mercury where volcano occurrence is strongly  
 182 associated with craters (Klimczak et al., 2018).

### 183 *3.2.3 Dike Propagation*

184 Once a fracture has formed, it will propagate if the forces trying to extend it ex-  
 185 ceed the forces resisting that extension. The fluid in the fracture is buoyant, generating  
 186 stresses which tend to elongate the dike. The stress from buoyancy grows with dike length,  
 187 so this force becomes more important in longer dikes. Strength in the host material serves  
 188 to limit growth, because fracturing at the tip of the dike is required for its extension (Ru-  
 189 bin, 1995). A compressional background stress increases the buoyancy required for a dike  
 190 to propagate. Crawford & Stevenson (1988) derive an expression for the minimum length  
 191 a dike must reach before pressure from melt buoyancy can fracture the crust and force  
 192 the crack to open further. A dike will propagate itself when

$$193 \quad K_c = (\pi l_{crit})^{1/2} [T + 2g\Delta\rho l_{crit}/\pi] \quad (4)$$

194 Here  $T$  is the local stress in the crust, defined here to be positive for tensile stress,  $K_c$   
 195 is the fracture toughness, and  $l_{crit}$  is the minimum length for a dike to become self prop-  
 196 agating. To propagate itself vertically against 100 kPa of compressive stress ( $\sim 5\%$  of what  
 197 faults can support), a dike would have to be 11 km long. If, on the other hand, there were  
 198 200 kPa of extensional stress, this critical length is less than 1 km. At  $T = 0$  the ex-

199 pression reduces to the result from Lister & Kerr (1991),

$$200 \quad l_{crit} = \left( \frac{K_c}{\Delta\rho g} \right)^{2/3} \approx 7 \text{ km} \quad (5)$$

201 Even modest compressional stresses therefore result in critical crack lengths larger  
 202 than the thickness of the entire crust. We thus conclude that the only time dike prop-  
 203 agation is likely to occur is immediately after a faulting event has reduced the local com-  
 204 pressional stress to approximately zero.

205 Dikes will be much more easily able to propagate if there is local tensile stress. There  
 206 are at least two ways to generate local tensile stress which we expect to be present. One  
 207 is impact craters. However, although we do not rule these out entirely, craters which are  
 208 sufficiently large to generate rebound and tensile stresses near the base of the crust are  
 209 likely to be uncommon. An alternative is for material to delaminate (i.e. detach and de-  
 210 scend as a diapir) from the base of the crust, imparting rapidly-changing stresses to the  
 211 material immediately above. Solid material tends to delaminate from the crust because  
 212 it is more dense than the melt immediately below it, and at the base of the crust tem-  
 213 peratures are high enough, and thus viscosities low enough, for material to flow. Delam-  
 214 ination has been discussed on Io (Kirchoff & McKinnon, 2009), as well as on metallic as-  
 215 teroids (Neufeld et al., 2019), and in the latter case is expected to recur on timescales  
 216 of a few tens of kyr. The stress will vary in and around the diapir, but Kirchoff & McK-  
 217 innon (2009) point out that its magnitude is roughly  $\sigma \sim \Delta\rho g \lambda$  where  $\lambda$  is the thick-  
 218 ness of the layer being shed.

219 Based on Neufeld et al. (2019), the diapirs will have a length scale of about 1 km.  
 220 Thus, delamination will generate stresses of order 100 kPa. Delamination also has the  
 221 advantage of being a recurrent phenomenon, so the base of the crust is constantly be-  
 222 ing stressed and unstressed.

223 Assuming fluid injection timescales of tens of kyr, the bottom 60% of the crust is  
 224 expected to be dominated by viscous processes, potentially leading to the growth of larger  
 225 intrusions than the initial dikes (cf. Karlstrom et al., 2017). Such intrusions, however,  
 226 would still be buoyant relative to the solid crust, and thus likely to ascend promptly (e.g.  
 227 as diapirs), rather than being stored.

### 228 **3.2.4 Dike Refreezing During Ascent**

229 Melt forced upward through a crack will lose heat to crack walls and eventually re-  
 230 freeze. For eruptions to occur, the timescale of freezing needs to be longer than the timescale  
 231 of melt ascent (e.g. Petford et al., 1994). Given the low viscosity of iron, the flow may  
 232 be turbulent, in which case for a dike of width  $D$  the ascent velocity is given by (Wil-  
 233 son & Head, 2017):

$$234 \quad u = \sqrt{D \frac{g \Delta\rho}{f_d \rho}} \quad (6)$$

235 where  $f_d$  is the coefficient of drag on the crack walls. To refreeze, we need the dike walls  
 236 to absorb a heat per area of  $D\rho L$ , where  $L$  is the latent heat of freezing. For eruption  
 237 timescale  $t$  and thermal diffusivity  $\kappa$ , this will propagate a distance  $\sqrt{\kappa t} = \sqrt{\kappa h/u}$  into  
 238 the walls, carrying away a heat per area of  $C_p \rho \Delta T \sqrt{\kappa t}$ , where  $C_p$  is the heat capacity  
 239 of the walls. Setting these equal gives the width of the smallest crack that will refreeze

$$240 \quad D_{min} = \left( \left( \underbrace{\frac{C_p \Delta T}{L}}_{\sim 10^{-1}} \right)^4 \underbrace{\frac{(\kappa h)^2}{g}}_{\sim 1 \text{ m}^5} \underbrace{f_d}_{\sim 10^{-1}} \underbrace{\frac{\rho}{\Delta\rho}}_{\sim 10^{1.5}} \right)^{1/5} \approx 0.3 \text{ m} \quad (7)$$

241 where here we have taken  $h=10$  km,  $g=0.1$  m s<sup>-2</sup>. This minimum width is similar to Earth,  
 242 where basalt has a minimum width of 1 meter (Rubin, 1995), so reasonable width cracks  
 243 are able to avoid refreezing. Assuming a viscosity of  $10^{-2}$  Pa · s, these values give us a  
 244 Reynolds number greater than  $10^3$ , so using the turbulent velocity is appropriate.

### 245 **3.3 Stage 3: Dike Closing, Reestablishing Compressional Regime**

#### 246 **3.3.1 Eruption Volume**

247 Eruptions are self-limiting processes, because compressional stress reaccumulates  
 248 as the liquid volume reduces and the crust subsides. An eruption will stop when the stress  
 249 in the crust is equal to the excess pressure in the ocean ( $gh\Delta\rho$ ). If, at the beginning of  
 250 an eruption, the difference between the ocean excess pressure and the local crustal stress  
 251 is  $P_{net}$ , then assuming the interior melt only compresses elastically (i.e. has zero volatile  
 252 content), a corresponding strain of  $\epsilon = \frac{P_{net}}{E}$  will accumulate. Treating the eruption as  
 253 a layer covering the entire body with thickness  $\delta$ , then  $\epsilon \approx \frac{\delta}{R}$ . If we assume that fault-  
 254 ing has relieved all compressional stress in the crust,  $P_{net} = gh\Delta\rho$  and

$$255 \quad \delta = \frac{gh\Delta\rho R}{E} = \frac{\frac{4}{3}\pi Gh\rho\Delta\rho R^2}{E} \quad (8)$$

$$256 \quad = 0.3 \text{ m} \times \left(\frac{\Delta\rho}{150 \text{ kg/m}^3}\right) \left(\frac{R}{100 \text{ km}}\right)^2 \left(\frac{h}{10 \text{ km}}\right) \left(\frac{10^{11} \text{ Pa}}{E}\right) \quad (9)$$

257 If some stress remains in the crust this value will be diminished somewhat. The nom-  
 258 inal value of  $\delta$  implies an eruption volume  $V_{erupt}$  of  $40 \text{ km}^3$ .

259 Eruptions will advect heat equal to  $V_{erupt} \rho(C_p\Delta T + L) \approx 10^{20}$  J. With a sur-  
 260 face thermal gradient of  $0.1 \text{ K/m}$  this is roughly 10 years of global conductive heat loss.  
 261 The importance of advection thus depends on how frequently those eruptions occur rel-  
 262 ative to this 10 year value.

#### 263 **3.3.2 Eruption Interval**

264 After an eruption, compressional crustal stress will be reestablished and the crust  
 265 will once again need to accumulate  $\sigma \approx \frac{\rho gh}{4} \approx \rho^2 hGR$  stress (as discussed in stage 2,  
 266 above) before this particular fault will fail again. New solid plated onto the base of the  
 267 crust with thickness  $\Delta h$ , will create a strain

$$268 \quad \epsilon = \frac{\Delta h \Delta\rho}{R \rho} \quad (10)$$

269 which can be rearranged to solve for the thickening required to cause the next failure

$$270 \quad \Delta h = \frac{\frac{\pi}{3}\rho^3 R^2 hG}{\Delta\rho E} \approx 150 \text{ m} \times \left(\frac{150 \text{ kg/m}^3}{\Delta\rho}\right) \left(\frac{R}{100 \text{ km}}\right)^2 \left(\frac{h}{10 \text{ km}}\right) \left(\frac{10^{11} \text{ Pa}}{E}\right) \quad (11)$$

271 Using  $\Delta t \approx \frac{2h\Delta h}{\kappa}$  we end up with failure every few kyr. The fact that this is large  
 272 compared to the 10 years above means that eruptions do not play a significant role in  
 273 the thermal evolution of the body.

274 This process differs from volcanic stress accumulation on Earth. On Earth, magma  
 275 chamber stresses can transition from elastic/brittle- to viscously-accommodated as the  
 276 thermal environment around the magma chamber changes (Jellinek & DePaolo, 2003).  
 277 In our case, stress arises from global volume changes associated with solidification, and  
 278 the thermal environment across the crust changes only very slowly: viscous relaxation  
 279 is always rapid at the base of the crust (Sec 3.2.2), and always negligible at the surface.



280 Note that in both of the previous sections we treated these processes as if all of the  
 281 planet’s stress accumulation and relief occurs on a single fault, which is certainly not the  
 282 case. In reality, faulting and erupting depends fundamentally on local stress evolution,  
 283 so global stress does not directly capture these events. The value of treating eruptions  
 284 this way is that it captures the relative volumes of erupted and deeply crystallized ma-  
 285 terial, and thus reflects the role of eruptions in the body’s overall thermal evolution.

### 286 3.3.3 Total Erupted Volume

287 A useful value to look at is the erupted layer thickness,  $\delta$ , divided by the thickness  
 288 of plating needed for eruption,  $\Delta h$ ,

$$289 \frac{\delta}{\Delta h} = \frac{\frac{4}{3}\pi Gh\rho\Delta\rho R^2/E}{\frac{\pi}{3}\rho^3 R^2 hG/\Delta\rho E} \quad (12)$$

$$290 = \left(2\frac{\Delta\rho}{\rho}\right)^2 \approx 10^{-3} \quad (13)$$

291 Importantly, most of the uncertain parameters that went into  $\delta$  and  $\Delta h$  cancel (note that  
 292 the  $E$  in the numerator and the denominator only cancel if the liquid and solid have sim-  
 293 ilar elastic moduli, which may not be the case in the presence of volatiles, as discussed  
 294 below). This means that although erupted volumes and frequencies are very uncertain,  
 295 the total amount of material that can be erupted is much better constrained. This value  
 296 is an upper limit, because it reflects the volume fraction of the body to participate in  
 297 eruptions if every faulting event relieves all local compressional stress and leads to an  
 298 eruption. The real value is likely to be smaller. One thousandth of the body as an up-  
 299 per limit on material erupted means that eruptions will not play a major role in ther-  
 300 mal and stress evolution, serving only to modify the surface. This is in contrast to, for  
 301 example, Io, where volcanism is the dominant source of heat transfer (e.g. Moore, 2001).

## 302 4 Role of Volatiles

303 There are two important ways that volatiles can alter the behavior of iron volcanism.  
 304 The first is the fact that they will be excluded from the crystallizing solid, making  
 305 the melt more buoyant than implied by just the phase transition and thermal contrac-  
 306 tion. Sulfur in particular is likely to be present (Chabot & Haack, 2006) and can be ex-  
 307 pected to play this role, but its concentration is a major unknown. In an extreme case,  
 308 native sulfur might erupt, in a similar manner to the sulfur volcanism proposed for Io  
 309 (Sagan, 1979; Williams et al., 2001), but eruption of an Fe-S alloy is much more likely.  
 310 Any light elements present in the melt should serve to enhance volcanism.

311 The second way that volatiles can be important parallels a role they play in sili-  
 312 cate magmatism, and likely play in cryovolcanism. As pressure is relieved during erup-  
 313 tions, volatiles may exsolve and form bubbles, lowering the density of the melt column,  
 314 accelerating its ascent and also increasing its compressibility (Bower & Woods, 1997).  
 315 This process is difficult to predict because it not only requires knowing the initial volatile  
 316 content of the iron, but also the tendency of those volatiles to exsolve. Further compli-  
 317 cating this is the fact that mantle stripping is a violent process (Asphaug et al., 2006)  
 318 which may have already exposed the bulk of the core to vacuum, removing volatiles which  
 319 could provide a bubble source. We therefore do not pursue this issue any further here.

## 320 5 Geomorphic Implications and Potential Constraints from Observa- 321 tion

322 Identifying iron volcanoes on metallic asteroids may prove to be challenging. Searches  
 323 for cryovolcanism motivate caution in interpreting features as volcanic in origin: Moore

324 & Pappalardo (2011) provide a summary of several past mistaken identifications of cry-  
 325 volcanism, an important warning for further searches for volcanoes. In addition, any  
 326 such volcanoes have had more than 4 billion years to be modified. 16 Psyche, for exam-  
 327 ple, is far from hydrostatic (Shepherd et al., 2017), and if not a rubble pile must at least  
 328 be heavily altered by impacts.

329 In the event that metallic volcanoes can be identified using present-day observa-  
 330 tions, they will likely be very informative. For example, it is likely that volcanoes will  
 331 be spatially associated with impact craters, analogous to what is seen on Mercury (Klim-  
 332 czak et al., 2018), and the degree of this association will inform the stress evolution of  
 333 the crust. A rapidly-cooling metallic flow may acquire a remanent magnetic field, if an  
 334 internal dynamo is active at that time (Bryson et al., 2015). Similarly, the style of vol-  
 335 canism on the body alone provides substantial insight. Because there is no analog to the  
 336 buoyant continental crust on Earth, the development of large mid-crustal magma cham-  
 337 bers and calderas is less likely on iron asteroids, so sill and lacolith formation are unlikely  
 338 to occur. However, if there is silicate material or a porous mega-regolith overlying the  
 339 bulk metallic crust, intrusive volcanism at the metal-silicate interface, perhaps leading  
 340 to diapirism, may occur. This situation is briefly addressed in Johnson et al. (2019) and  
 341 warrants further work. If the volcanism is effusive, we expect it to form thin, laterally-  
 342 extensive deposits as a result of liquid iron’s low viscosity (Griffiths, 2000). If the vol-  
 343 canism is explosive, the eruptive behavior will depend on the volatiles present and the  
 344 reservoir conditions (Bower & Woods, 1997; Lu & Kieffer, 2009) and will have major im-  
 345 plications for light element incorporation in cores, volatile retention during mantle strip-  
 346 ping, and devolatilization during subsequent evolution. We caution, however, that in the  
 347 latter case the eruption velocity could easily exceed the escape velocity ( $\approx 200$  m/s) mak-  
 348 ing identification of volcanic deposits more challenging than on e.g. Mercury.

## 349 **6 Evidence in the Meteorite Record**

350 A key prediction that follows from metallic volcanism is that bodies hosting it will  
 351 have two end-member types of solids which experienced very different histories. Mate-  
 352 rial crystallizing onto the bottom of the crust will cool slowly and will exhibit an inverse  
 353 correlation between cooling rate and light element content. Erupted material will crys-  
 354 tallize very quickly, and unless it is reheated will show  $\sim$ instantaneous cooling. This quen-  
 355 ching will prevent elemental fractionation, so erupted material will record the (non-volatile)  
 356 element abundances of the liquid interior at the time it was erupted. Incompatible el-  
 357 element (Ga, Ge, Ir, etc.) concentrations will be much larger than contemporaneously formed  
 358 deep solids. These meteorites would likely be some of the most incompatible element en-  
 359 riched material in their meteorite family. If volatile exsolution is involved, the quenched  
 360 solids would likely contain vesicles. However, because erupted material is a small vol-  
 361 ume fraction of the body, the quenched meteorites will likely be rare. Although a detailed  
 362 analysis is beyond the scope of this paper, it is plausible that the modern meteorite record  
 363 can serve as a test of this paper’s predictions.

364 It is important to note that there are important differences between how silicate  
 365 and iron cooling and crystallization are recorded in hand specimens. Most of the visi-  
 366 ble texture in iron meteorites is the result of sub-solidus processes (Hutchison, 2004; Was-  
 367 son, 1985), which can be used to determine cooling rates (Sec 1). Chemical and/or tex-  
 368 tural evidence of crystallization itself (e.g. dendrites) may be retained, but is predicted  
 369 to vary on length-scales much larger than almost all available iron meteorite specimens  
 370 (Haack & Scott, 2009), so no spatial information on crystallization is available.

## 371 **7 Conclusions**

372 We predict that some metallic asteroids will have hosted volcanic activity while so-  
 373 lidifying. Overall, metallic volcanism should bear more resemblance to silicate volcan-

374 ism than cryovolcanism. This is because, like silicates, the melt is buoyant, and the ther-  
 375 mal conditions under which melt travels through dikes are similar. However, fracture ini-  
 376 tiation is more difficult in metallic systems because of the ductility and tensile strength  
 377 of iron, while fracture growth is opposed by the large fracture toughness of iron and the  
 378 background compressional environment. Apart from volatiles, the largest uncertainty in  
 379 our analysis probably relates to dike initiation and propagation. This depends on the  
 380 somewhat uncertain fracture toughness of the crust (Ashby, 1999), and the frequency  
 381 of large enough stresses to cause fracturing and fracture propagation. At a minimum,  
 382 large impacts should be able to cause the crust to occasionally fail, but if delamination  
 383 occurs, it is more likely to drive dike propagation and ferrovulcanism.

384 The details of the hypothesized processes will require substantial further theoret-  
 385 ical investigation. Geomorphological examples of iron volcanoes would make for partic-  
 386 ularly striking confirmation, but will likely be very difficult, if not impossible, to unam-  
 387 biguously identify. More likely, testing of this hypothesis will come from the meteorite  
 388 record, either by explaining existing anomalies in the record or predicting the charac-  
 389 teristics of future meteorites.

**Table 1.** Parameters Used

	Description	Value	Source
$\kappa_s$	Silicate thermal diffusivity	$1.1 \times 10^{-6} \text{ m}^2/\text{s}$	(Carslaw & Jaeger, 1959)
$\kappa_m$	Metal thermal diffusivity	$1.2 \times 10^{-5} \text{ m}^2/\text{s}$	(Carslaw & Jaeger, 1959)
$T_m$	Melting point	1200 K	Assumed
$T_s$	Temperature due to solar irradiation	200 K	Assumed
$L$	Latent heat	$2.7 \times 10^5 \text{ J/kg}$	(Haack et al., 1990)
$C_p$	Specific heat capacity	$569 \text{ J/kg}\cdot\text{K}$	(Carslaw & Jaeger, 1959)
$Q$	Activity energy	$2.5 \times 10^5 \text{ J/mol}$	(Frost & Ashby, 1982)
$R_g$	Gas constant	$8.314 \text{ J/mol}\cdot\text{K}$	
$R$	Body Radius	100 km	Assumed
$g$	Acceleration due to gravity	$[\text{m}/\text{s}^2]$	
$\rho$	Density	$7400 \text{ km}/\text{m}^3$	(Carslaw & Jaeger, 1959)
$\Delta\rho$	Density contrast between melt and solid	$\approx \rho/40$	Assumed, very approximate
$h$	Crust thickness	$[\text{m}]$	
$h_e$	Elastic/brittle crustal layer thickness	$h/2$	Calculated, approximate
$P$	Pressure	$[\text{Pa}]$	
$f_s$	Coefficient of friction on faults	0.65	(Turcotte & Schubert, 2014)
$f$	Drag coefficient in dikes	0.1	Assumed
$\sigma$	Stress	$[\text{Pa}]$	
$\epsilon$	Strain	dimensionless	
$\dot{\epsilon}$	Strain Rate	$[\text{s}^{-1}]$	
$K$	Bulk Modulus	$10^{11} \text{ Pa}$	(Ahrens & Johnson, 1995)
$K_c$	Fracture Toughness	$10^7 \text{ Pa}\cdot\text{m}^{1/2}$	(Ashby, 1999, Figure 4.7)
$D$	Dike width	$[\text{m}]$	
$\Delta h$	Crystallized layer thickness	$[\text{m}]$	
$\delta$	Erupted layer thickness if global	$[\text{m}]$	
$l_{crit}$	Dike Critical Length	$[\text{m}]$	(Crawford & Stevenson, 1988)
$\lambda$	Diapir Thickness	$[\text{m}]$	

Note that entries without values or without sources are outputs we are finding. Brackets indicate units when a specific value is not relevant.

## References

- Ahrens, T. J., & Johnson, M. L. (1995). Shock wave data for minerals. *Mineral Physics & Crystallography: A Handbook of Physical Constants*, 2, 143-184.
- Albarède, F., Bouchet, R. A., & Blichert-Toft, J. (2013). Siderophile elements in IVA irons and the compaction of their parent asteroidal core. *Earth and Planetary Science Letters*, 362, 122-129. <https://doi.org/10.1016/j.epsl.2012.11.059>
- Ashby, M. F. (1999), *Materials selection in mechanical design*, Butterworth-Heinemann, Oxford, England.
- Asphaug, E., Agnor, C. B., & Williams, Q. (2006) Hit and run planetary collisions. *Nature*, 438, 155-160. <https://doi.org/10.1038/nature04311>
- Bottke, W. F., Durda, D. D., Nesvorný, D., Jedicke, R., Morbidelli, A., Vokrouhlický, D., Levison, H. F. (2005). Linking the collisional history of the main asteroid belt to its dynamical excitation and depletion. *Icarus*, 179, 63-94. <https://doi.org/10.1016/j.icarus.2005.05.017>
- Bower, S. M. & Woods, A. W. (1997). Control of magma volatile content on the mass erupted during explosive volcanic eruptions Saturated magma. *Journal of Geophysical Research*, 102, 10273-10290. <https://doi.org/10.1029/96JB03176>
- Bryson, J. F. J., Nichols, C. I. O., Herrero-Albillos, J., Kronast, F., Kasama, T., Alimadadi, H., ... Harrison, R. J. (2015). Long-lived magnetism from solidification-driven convection on the pallasite parent body. *Nature*, 517(7535), 472-475. <https://doi.org/10.1038/nature14114>
- Carlslaw, H. S., & Jaeger, J. C. (1959). *Conduction of heat in solids*. Oxford Science Publications (p. 497). Oxford, England.
- Chabot, N. L., & Haack, H. (2006). *Evolution of Asteroidal Cores. Meteorites and the Early Solar System II*, University of Arizona Press, 747-771.
- Crawford, G. D., & Stevenson, D. J. (1988). Gas-driven water volcanism and the resurfacing of Europa. *Icarus*, 73(1), 66-79. [https://doi.org/10.1016/0019-1035\(88\)90085-1](https://doi.org/10.1016/0019-1035(88)90085-1)
- Frost, H. J., & Ashby, M. F. (1982), *Deformation-mechanism maps: The plasticity and creep of metals and ceramics*, Pergamon Press, Oxford, England.
- Fulton, P. M., Brodsky, E. E., Kano, Y., Mori, J., Chester, F., Ishikawa, T., et al. (2013). Low coseismic friction on the Tohoku-Oki fault determined from temperature measurements. *Science*, 342(6163), 1214-1217. <https://doi.org/10.1126/science.1243641>
- Goldstein, J. I., Scott, E. R. D., & Chabot, N. L. (2009). Iron meteorites: Crystallization, thermal history, parent bodies, and origin. *Chemie Der Erde*, 69(4), 293-325. <https://doi.org/10.1016/j.chemer.2009.01.002>
- Griffiths, R. W. (2000). The dynamics of lava flows. *Annual Review of Fluid Mechanics*, 32, 477-518. <https://doi.org/10.1146/annurev.fluid.32.1.477>
- Haack, H., Rasmussen, K. L., & Warren, P. H. (1990), Effects of regolith/megaregolith insulation on the cooling histories of differentiated asteroids, *J. Geophys. Res.*, 95(B4), 5111-5124, doi: 10.1029/JB095iB04p05111
- Haack, H., Scott, E. R. D. (2009). Asteroid core crystallization by inward dendritic growth. *Journal of Geophysical Research*, 97(E9), 14727-14734. <https://doi.org/10.1029/92je01497>
- Head, J. W., & Wilson, L. (1992). Lunar mare volcanism: Stratigraphy, eruption conditions, and the evolution of secondary crusts. *Geochimica et Cosmochimica Acta*, 56(6), 2155-2175. [https://doi.org/10.1016/0016-7037\(92\)90183-J](https://doi.org/10.1016/0016-7037(92)90183-J)
- Hevey, P. J., & Sanders, I. S. (2006). A model for planetesimal meltdown by  $^{26}\text{Al}$  and its implications for meteorite parent bodies. *Meteoritics & Planetary Science*, 41(1), 95-106. <https://doi.org/10.1111/j.1945-5100.2006.tb00195>
- Hutchison, R. (2004), *Meteorites: A petrologic, chemical and isotopic synthesis*. Cambridge Univ. Press, Cambridge, England.
- Jellinek, A. M., & DePaolo, D. J. (2003). A model for the origin of large silicic magma chambers: Precursors of caldera-forming eruptions. *Bulletin of Vol-*

- canology, 65(5), 363-381. <https://doi.org/10.1007/s00445-003-0277-y>
- 445 Jellinek, A. M., & Kerr, R. C. (2001). Magma dynamics, crystallization, and  
 446 chemical differentiation of the 1959 Kilauea Iki lava lake, Hawaii, revisit-  
 447 ed. *Journal of Volcanology and Geothermal Research*, 110(3-4), 235-263.  
 448 [https://doi.org/10.1016/S0377-0273\(01\)00212-8](https://doi.org/10.1016/S0377-0273(01)00212-8)
- 449 Johnson, B. C., Sori, M. M., & Evans, A. J. (2019). Ferrovulcanism, Pallasites, and  
 450 Psyche. *Lunar and Planetary Science Conference L*, abstract #1625.
- 451 Karlstrom, L., Paterson, S. R., & Jellinek, A. M. (2017). A reverse energy cas-  
 452 cade for crustal magma transport. *Nature Geoscience*, 10(8), 604-608.  
 453 <https://doi.org/10.1038/NGEO2982>
- 454 Karlstrom, L., & Richards, M. (2011). On the evolution of large ultramafic magma  
 455 chambers and timescales for flood basalt eruptions. *Journal of Geophysical*  
 456 *Research: Solid Earth*, 116(8), 1-13. <https://doi.org/10.1029/2010JB008159>
- 457 Kirchoff, M. R., & McKinnon, W. B. (2009). Formation of mountains on  
 458 Io: Variable volcanism and thermal stresses. *Icarus*, 201(2), 598-614.  
 459 <https://doi.org/10.1016/j.icarus.2009.02.006>
- 460 Klimczak, C., Crane, K. T., Habermann, M. A., & Byrne, P. K. (2018). The spatial  
 461 distribution of Mercury's pyroclastic activity and the relation to lithospheric  
 462 weaknesses. *Icarus*, 315, 115-123. <https://doi.org/10.1016/j.icarus.2018.06.020>
- 463 Lister, J. R., & Kerr, R. C. (1991). Fluid-mechanical models of crack propagation  
 464 and their application to magma transport in dykes. *Journal of Geophysical*  
 465 *Research*, 96(B6), 10049-10077. <https://doi.org/10.1029/91JB00600>
- 466 Lopes, R.M.C. & Gregg, T.K.P (2004). *Volcanic worlds: Exploring the solar sys-*  
 467 *tem's volcanoes*, Springer, 235.
- 468 Lord, P., Tilley, S., Oh, D. Y., Goebel, D., Polanskey, C., Snyder, S., ... Elkins-  
 469 Tanton, L. (2017). Psyche: Journey to a metal world. *IEEE Aerospace Confer-*  
 470 *ence Proceedings*, 2014, 1-11. <https://doi.org/10.1109/AERO.2017.7943771>
- 471 Lu, X., & Kieffer, S. W. (2009). Thermodynamics and mass transport  
 472 in multicomponent, multiphase H<sub>2</sub>O Systems of Planetary Inter-  
 473 est. *Annual Review of Earth and Planetary Sciences*, 37(1), 449-477.  
 474 <https://doi.org/10.1146/annurev.earth.031208.100109>
- 475 Manga, M., & Wang, C. Y. (2007). Pressurized oceans and the eruption of liquid  
 476 water on Europa and Enceladus. *Geophysical Research Letters*, 34(7), 1-5.  
 477 <https://doi.org/10.1029/2007GL029297>
- 478 Matter, A., Delbo, M., Carry, B., & Ligori, S. (2013). Evidence of a  
 479 metal-rich surface for the Asteroid (16) Psyche from interferomet-  
 480 ric observations in the thermal infrared. *Icarus*, 226(1), 419-427.  
 481 <https://doi.org/10.1016/j.icarus.2013.06.004>
- 482 Melosh, H. J. (1989). *Impact cratering, a geologic process*. Oxford Univ. Press, New  
 483 York, United States.
- 484 Moore, W.B. (2001). The thermal state of Io. *Icarus* 154, 548-550.  
 485 <https://doi.org/10.1006/icar.2001.6739>
- 486 Moore, J. M., & Pappalardo, R. T. (2011). Titan: An exogenic world? *Icarus*,  
 487 212(2), 790-806. <https://doi.org/10.1016/j.icarus.2011.01.019>
- 488 Moore, J. M., McKinnon, W.B., Spencer, J.R. et al. (2016). The geology of Pluto  
 489 and Charon through the eyes of New Horizons, *Science* 351, 1284-1293.  
 490 <https://doi.org/10.1126/science.aad7055>
- 491 Neeley, J. R., Clark, B. E., Ockert-Bell, M. E., Shepard, M. K., Conklin, J.,  
 492 Cloutis, E. A., ... & Bus, S. J. (2014). The composition of M-type asteroids  
 493 II: Synthesis of spectroscopic and radar observations. *Icarus*, 238, 37-50.  
 494 <https://doi.org/10.1016/j.icarus.2014.05.008>
- 495 Neufeld, J. A., Bryson, J. F. J., & Nimmo, F. (2019). The top-down solidification  
 496 of iron asteroids driving dynamo evolution. *Journal of Geophysical Research:*  
 497 *Planets*. In review.

- 499 Nimmo, F., & Spencer, J.R. (2015). Powering Triton's recent geological activ-  
500 ity by obliquity tides: Implications for Pluto geology, *Icarus* 246, 2-10.  
501 <https://doi.org/10.1016/j.icarus.2014.01.044>
- 502 Petford, N., Kerr, R. C., & Lister, J. R. (1993). Dike transport of grani-  
503 toid magmas. *Geology*, 21(9), 845-848. [https://doi.org/10.1130/0091-7613\(1993\)021;0845:DTOGM;2.3.CO;2](https://doi.org/10.1130/0091-7613(1993)021;0845:DTOGM;2.3.CO;2)
- 504 Porco, A. C. C., Helfenstein, P., Thomas, P. C., Ingersoll, A. P., Wisdom, J., West,  
505 R., ... Johnson, V. T. (2006). Cassini observes the active south pole of Ence-  
506 ladus, 311, 1393-1401. <https://doi.org/10.1126/science.1123013>
- 507 Roth, L., Saur, J., Retherford, K. D., Strobel, D. F., Feldman, P. D., McGrath,  
508 M. A., & Nimmo, F. (2014). Transient water vapor at Europa's south pole.  
509 *Science*, 343(6167), 171-174. <https://doi.org/10.1126/science.1247051>
- 510 Rubin, A. M. (1995). Propagation of Magma-Filled Cracks. *Annual Reviews*, 215-  
511 217. <https://doi.org/10.1146/annurev.ea.23.050195.001443>
- 512 Rubin, A. M. (1998). Dike ascent in partially molten rock. *Journal of Geophysical*  
513 *Research: Solid Earth*, 103, 20901-20919. <https://doi.org/10.1029/98JB01349>
- 514 Sagan, C. (1979). Sulphur flows on Io. *Nature*, 280, 750-753.  
515 <https://doi.org/10.1038/280750a0>
- 516 Scheinberg, A., Elkins-Tanton, L. T., Schubert, G., & Bercovici, D. (2016).  
517 Core solidification and dynamo evolution in a mantle-stripped plan-  
518 etesimal. *Journal of Geophysical Research: Planets*, 121(1), 2-20.  
519 <https://doi.org/10.1002/2015JE004843>
- 520 Schenk, P.M., McKinnon, W.B., Gwynn, D., Moore, J.M. (2001) Flooding of  
521 Ganymede's bright terrains by low-viscosity water-ice lavas, *Nature* 410, 56-  
522 60. <https://doi.org/10.1038/35065027>
- 523 Shepherd, M. K., Richardson, J., Taylor, P. A., Rodrigues-Ford, L. A., Conrad, A.  
524 de Pater, I., et al. (2017). Radar observations and shape model of asteroid 16  
525 Psyche. *Icarus*, 281, 388-403. <https://doi.org/10.1016/j.icarus.2016.08.011>
- 526 Tkalcic, B.J., Golabek, G.J., Brenker, F., (2013). Solid-state plastic deformation in  
527 the dynamic interior of a differentiated asteroid, *Nature Geoscience*. 6, 93-97.  
528 <https://doi.org/10.1038/ngeo1710>
- 529 Turcotte, D. L., & G. Schubert (2014), *Geodynamics*, Cambridge Univ. Press, Cam-  
530 bridge, England.
- 531 Wasson, J. T., *Meteorites: Their Record of Early Solar-System History*, 267, W.H.  
532 Freeman Press, New York, 1985.
- 533 Williams, D. A., Greeley, R., Lopes, R. M. C., & Davies, A. G. (2001). Evalua-  
534 tion of sulfur flow emplacement on Io from Galileo data and numerical mod-  
535 eling. *Journal of Geophysical Research E: Planets*, 106(E12), 33161-33174.  
536 <https://doi.org/10.1029/2000JE001340>
- 537 Williams, Q. (2009). Bottom-up versus top-down solidification of the cores of small  
538 solar system bodies: Constraints on paradoxical cores. *Earth and Planetary*  
539 *Science Letters*, 284(3-4), 564-569. <https://doi.org/10.1016/j.epsl.2009.05.019>
- 540 Wilson, L. (2009). Volcanism in the solar system, *Nature Geosci.* 2, 389-397.  
541 <https://doi.org/10.1038/ngeo529>
- 542 Wilson, L., & Head, J.W. (2017). Generation, ascent and eruption of magma  
543 on the Moon: New insights into source depths, magma supply, intrusions  
544 and effusive/explosive eruptions (Part 1: Theory), *Icarus* 283, 146-175.  
545 <https://doi.org/10.1016/j.icarus.2015.12.039>
- 546 Yang, J., Goldstein, J. I., & Scott, E. R. D. (2008). Metallographic cooling rates  
547 and origin of IVA iron meteorites. *Geochimica et Cosmochimica Acta*, 72,  
548 3043-3061. <https://doi.org/10.1016/j.gca.2008.04.009>
- 549 Yang, J., & Goldstein, J. I. (2006). Metallographic cooling rates of the IIIAB  
550 iron meteorites. *Geochimica et Cosmochimica Acta*, 70(12), 3197-3215.  
551 <https://doi.org/10.1016/j.gca.2006.04.007>

553 Yang, J., Goldstein, J. I., & Scott, E. R. D. (2007). Iron meteorite evidence for early  
554 formation and catastrophic disruption of protoplanets. *Nature*, 446, 888-891.  
555 <https://doi.org/10.1038/nature05735>

## 556 **Acknowledgments**

557 Partial support from NASA-80NSSC18K0601 is acknowledged. The MS was orig-  
558 inally submitted on 28 Nov 2018. We thank the reviewers, Dave Williams and Mark Jellinek,  
559 for their perceptive comments, and Denton Ebel for helpful advice on meteorite textures.  
560 This is a theoretical paper and no data were generated.